



NDUFS4 deletion triggers loss of NDUF12 in *Ndufs4*^{-/-} mice and Leigh syndrome patients: A stabilizing role for NDUF2

Merel J.W. Adjubo-Hermans^a, Ria de Haas^b, Peter H.G.M. Willems^a, Aleksandra Wojtala^c, Sjenet E. van Emst-de Vries^a, Jori A. Wagenaars^a, Mariel van den Brand^b, Richard J. Rodenburg^b, Jan A.M. Smeitink^b, Leo G. Nijtmans^{b,1}, Leonid A. Sazanov^d, Mariusz R. Wieckowski^{c,*}, Werner J.H. Koopman^{a,**}

^a Department of Biochemistry, Radboud Institute for Molecular Life Sciences, Radboud Center for Mitochondrial Medicine, Radboudumc, Nijmegen, the Netherlands

^b Department of Pediatrics, Radboud Center for Mitochondrial Medicine, Radboudumc, Nijmegen, the Netherlands

^c Nencki Institute of Experimental Biology, Warsaw, Poland

^d Institute of Science and Technology, Klosterneuburg, Austria

ARTICLE INFO

Keywords:

NADH:ubiquinone oxidoreductase
Leigh syndrome
Proteomics
Fibroblasts

ABSTRACT

Mutations in *NDUFS4*, which encodes an accessory subunit of mitochondrial oxidative phosphorylation (OXPHOS) complex I (CI), induce Leigh syndrome (LS). LS is a poorly understood pediatric disorder featuring brain-specific anomalies and early death. To study the LS pathomechanism, we here compared OXPHOS proteomes between various *Ndufs4*^{-/-} mouse tissues. *Ndufs4*^{-/-} animals displayed significantly lower CI subunit levels in brain/diaphragm relative to other tissues (liver/heart/kidney/skeletal muscle), whereas other OXPHOS subunit levels were not reduced. Absence of *NDUFS4* induced near complete absence of the *NDUF12* accessory subunit, a 50% reduction in other CI subunit levels, and an increase in specific CI assembly factors. Among the latter, *NDUF2* was most highly increased. Regarding *NDUFS4*, *NDUF12* and *NDUF2*, identical results were obtained in *Ndufs4*^{-/-} mouse embryonic fibroblasts (MEFs) and *NDUFS4*-mutated LS patient cells. *Ndufs4*^{-/-} MEFs contained active CI *in situ* but blue-native-PAGE highlighted that *NDUF2* attached to an inactive CI subcomplex (CI-830) and inactive assemblies of higher MW. In *NDUF12*-mutated LS patient cells, *NDUF12* absence did not reduce *NDUFS4* levels but triggered *NDUF2* association to active CI. BN-PAGE revealed no such association in LS patient fibroblasts with mutations in other CI subunit-encoding genes where *NDUF2* was attached to CI-830 (*NDUFS1*, *NDUFV1* mutation) or not detected (*NDUFS7* mutation). Supported by enzymological and CI *in silico* structural analysis, we conclude that absence of *NDUFS4* induces near complete absence of *NDUF12* but not *vice versa*, and that *NDUF2* stabilizes active CI in *Ndufs4*^{-/-} mice and LS patient cells, perhaps in concert with mitochondrial inner membrane lipids.

1. Introduction

Mitochondrial complex I (CI or NADH:ubiquinone oxidoreductase; EC 1.6.5.3) is the first and largest (~1 MDa) complex of the oxidative phosphorylation (OXPHOS) system, which further consists of four other

multi-subunit complexes (CII-CV; [1]). CI transfers electrons from NADH to ubiquinone and uses the energy released by this process to convey protons (H⁺) from the mitochondrial matrix across the mitochondrial inner membrane (MIM). This process contributes to establishment of a trans-MIM proton-motive force (PMF) that is used to

Abbreviations: BN-PAGE, blue-native polyacrylamide gel electrophoresis; CI-V, complex I to V; CNS, Central Nervous System; KO, knockout; LS, Leigh Syndrome; MEFs, mouse embryonic fibroblasts; MIM, mitochondrial inner membrane; *NDUF12*, NADH-ubiquinone oxidoreductase subunit A12; *NDUF2*, NADH-ubiquinone oxidoreductase complex assembly factor 2; *NDUFS4*, NADH-ubiquinone oxidoreductase Fe-S protein 4; OXPHOS, oxidative phosphorylation; SDS-PAGE, sodium dodecyl sulfate polyacrylamide gel electrophoresis; WT, wild-type

* Correspondence to: M.R. Wieckowski, Nencki Institute of Experimental Biology, Pasteur 3, Warsaw, Poland.

** Correspondence to: W.J.H. Koopman, Department of Biochemistry (286), Radboud Institute for Molecular Life Sciences (RIMLS), Radboud University Medical Centre (Radboudumc), P.O. Box 9101, NL-6500 HB Nijmegen, the Netherlands.

E-mail addresses: m.wieckowski@nencki.gov.pl (M.R. Wieckowski), werner.koopman@radboudumc.nl (W.J.H. Koopman).

¹ Deceased 1 May 2018.

<https://doi.org/10.1016/j.bbambio.2020.148213>

Received 4 February 2020; Received in revised form 15 April 2020; Accepted 16 April 2020

Available online 23 April 2020

0005-2728/© 2020 The Author(s). Published by Elsevier B.V. This is an open access article under the CC BY license

(<http://creativecommons.org/licenses/by/4.0/>).

generate ATP by chemiosmotic coupling [2]. CI consists of three functional modules [3]: the N-module (NADH binding and oxidation), the Q-module (electron transfer to ubiquinone) and the P-module (proton pumping). Structurally, CI is L-shaped and consists of 45 subunits, one of which (NDUFAB1) occurs twice in the fully assembled complex [4,5]. For its catalytic activity CI requires 14 core proteins [6], half of which is encoded by the mitochondrial DNA (mtDNA: MTND1, MTND2, MTND3, MTND4, MTND4L, MTND5, MTND6) and the remainder by the nuclear DNA (nDNA: NDUFV1, NDUFV2, NDUFS1, NDUFS2, NDUFS3, NDUFS7, NDUFS8). In addition to this catalytic core, CI contains 30 currently-identified nDNA-encoded accessory subunits of largely unknown function [7]. Biogenesis of CI is assisted by at least 14 nDNA-encoded assembly factors and the current evidence suggests that its assembly occurs by a mechanism in which five CI protein modules are pre-formed (N, Q/Pp-a, Pp-b, Pd-a and Pd-b) and subsequently combined [8]. The structural and functional architecture of CI was described at various levels of detail in diverse biological models like the yeast *Y. lipolytica*, the eubacterium *Thermus thermophilus*, bovine heart, ovine heart and porcine heart [4,9–14]. At a higher level of organization, CI forms a supramolecular assembly with CIII and CIV [15], the structure and potential functional aspects of which were presented [13,16–19].

Mutations in CI structural subunits induce isolated CI deficiency (OMIM 252010) and are primarily associated with Leigh syndrome (LS; [20,21]). This syndrome is generally characterized by neurodegeneration, variable symptoms, mitochondrial dysfunction and bilateral CNS lesions [22]. The *NDUFS4* gene encodes the 18-kDa NDUFS4 (NADH-ubiquinone oxidoreductase Fe-S protein 4) accessory subunit of CI, which plays an important role during CI assembly and in CI stability [23–27]. At the clinical level, *NDUFS4* mutations primarily affect the brainstem, basal ganglia and (less frequently) the cerebral cortex and are typically associated with hypotonia, abnormal ocular movements, visual impairment, psychomotor arrest/regression and episodes of respiratory failure [28]. On average, mutations in the *NDUFS4* subunit induce a 50% reduction of CI activity in patient fibroblasts and cause death within 10 months after birth [28].

Various *Ndufs4*^{-/-} mouse models have been generated to study the LS pathomechanism and aid the development of therapeutic strategies [29,30]. For instance, whole-body *Ndufs4*^{-/-} mice present with many of the clinical features observed in LS patients and are widely used. These KO animals display an isolated CI enzymatic deficiency, appear healthy until 5 weeks after birth but die at ~7 weeks [31–33]. Interestingly, mice with a specific knockout of *Ndufs4* in neurons and glia cells (NesKO mice) displayed a phenotype very similar to that of whole-body KO mice, including progressive neuronal deterioration and gliosis with early involvement of the olfactory bulb, cerebellum, and vestibular nuclei [34,35]. Specific knockout of *Ndufs4* in midbrain dopaminergic (DA) neurons did not induce neurodegeneration, loss of striatal innervation or obvious Parkinson's disease (PD) symptoms [36]. However, DA homeostasis was abnormal and *Ndufs4*^{-/-} DA neurons were more vulnerable to the neurotoxin 1-methyl-4-phenyl-1,2,3,6-tetrahydropyridine (MPTP), suggesting that CI deficiency might contribute to PD pathophysiology [36]. The latter study also revealed that heart-specific *Ndufs4* knockout induces only a mild CI deficiency *in vivo*. The above results, combined with the fact that: (1) lifespan was not affected in heart-specific *Ndufs4*^{-/-} mice [36,37] and (2) whole-body KO and NesKO mice displayed near identical clinical phenotypes [34], suggest that the clinical phenotype associated with *Ndufs4* KO is primarily due to brain abnormalities [38]. In this sense, evidence was provided that lesions within the dorsal brain stem vestibular nucleus (VN) and deep cerebellar fastigial nucleus (FN) contribute to dysregulation of the central respiratory network, leading to respiratory failure and death of *Ndufs4* KO mice [35]. To gain insight into the pathomechanism of *Ndufs4* gene deletion, we applied for the first time quantitative mass spectrometry to determine the levels of OXPHOS subunits and assembly factors in various tissues from whole-body *Ndufs4*^{-/-} mice (brain,

liver, heart, kidney, diaphragm, skeletal muscle) and analyzed LS patient cells harboring nDNA-encoded CI mutations (*NDUFS1*, *NDUFS4*, *NDUFS7*, *NDUFV1*, *NDUFA12*, *NDUFAF2*). We demonstrate that *Ndufs4* gene deletion reduces CI subunit levels and propose that *NDUFAF2* and possibly MIM lipids can stabilize active CI at the cellular level.

2. Materials and methods

2.1. Animal breeding, tissue dissection and proteomics analysis

Initial breeding pairs of heterozygous *Ndufs4*^{+/-} mice [31] were kindly donated by the Palmiter laboratory (Howard Hughes Medical Institute, University of Washington, Seattle). Mice were group-housed at the Central Animal Facility (CDL) of the Radboud University at 22 °C with a day/night rhythm of 12 h. The animals had *ad libitum* access to food and water and were fed on a standard animal diet (V1534-300 R/M-H; Ssniff GmbH, Soest, Germany). *Ndufs4* whole-body knockout (*Ndufs4*^{-/-}; KO) and wild-type (WT) mice were generated by crossing heterozygote males and females as described previously [31,39]. The genotype of the mice was confirmed by polymerase chain reaction. Animal experiments were approved by the Committee for Animal Experiments of the Radboud University Nijmegen Medical Center Nijmegen, The Netherlands, in accordance with Dutch laws and regulations and performed under the guidelines and regulations of the Dutch Council for Animal Care. For proteomics analysis, three WT mice (2 male, 1 female) and three KO (*Ndufs4*^{-/-}) mice (2 male, 1 female) were sacrificed 6 weeks after birth by decapitation. Different tissues were isolated and extensively washed in PBS and stored in liquid nitrogen. In case of the brain, a slice (1–1.5 mm thickness) was manually dissected and contained parts of the following brain areas: cerebral cortex, hippocampal formation, thalamus, hypothalamus, internal capsule, optic tract and the amygdala (Allen mouse brain atlas; <http://mouse.brain-map.org/>). For comparison, other organs (from 1 KO and 1 WT animal; both males) were included in the proteomics analysis: liver, kidney, diaphragm, heart, and skeletal muscle from the hind leg (containing: *musculus vastus medialis*, *musculus gracilis*, *rectus femoris*, *musculus biceps femoris*, *musculus semitendinosus*, *musculus semimembranosus* and *musculus adductor*). All tissues were extensively washed in PBS and stored for further studies in liquid nitrogen. Liquid chromatography-MS3 spectrometry (LC-MS/MS) was carried out at the Thermo Fisher Center for Multiplexed Proteomics (Dept. of Cell Biology, Harvard Medical School, Cambridge, MA, USA). Peptide fractions were analyzed using an LC-MS3 data collection strategy on an Orbitrap Fusion mass spectrometer (Thermo Fisher Scientific Inc., Waltham, MA, USA). A detailed description of the proteomics analysis is provided in the Supplement. Cluster analysis of the complete detected proteome (6551 proteins) demonstrated that the WT and KO animals clustered in two distinct groups (data not shown). In this study we focused on the OXPHOS system. The remainder of the proteomics data will be presented in a follow-up manuscript (in preparation).

2.2. Mouse embryonic fibroblasts

Immortalized mouse embryonic fibroblasts (MEFs) of *Ndufs4* KO and WT mice were generated previously [40]. MEFs were cultured at 37 °C in a humidified atmosphere (95% air and 5% CO₂) in DMEM medium (#10938, Invitrogen, Carlsbad, CA, USA), containing 25 mM D-glucose and supplemented with L-glutamine (4 mM), sodium pyruvate (1 mM), 10% (v/v) Fetal Calf Serum (FCS, Greiner Bio-one, Frickhausen, Germany) and 0.1% (v/v) Gentamycin (Invitrogen).

2.3. Primary human skin fibroblasts

Human Fibroblasts were obtained following informed parental consent and according to the relevant Institutional Review Boards from skin biopsies of a healthy individual (CT5120) and various patients (P)

with complex I (CI) deficiency (OMIM 252010). Control and patient fibroblasts were previously characterized at the genetic, biochemical and cellular level (e.g. [41–44]). All patients displayed an isolated CI deficiency in muscle tissue and cultured fibroblasts and were negative with respect to mitochondrial DNA (mtDNA) alterations previously associated with CI deficiency. Patient cell lines (Supplementary Table S1) harbored mutations in various CI structural subunits: *NDUFS7* (S7-P5175), *NDUFV1* (V1-P5866), *NDUFA12* (A12), *NDUFS1* (S1-P6173) and *NDUFS4* (S4-P4608, S4-P5260). Also a patient with a mutation in the CI assembly factor *NDUFAF2* (AF2-P8872) was included. Fibroblasts were cultured in Medium 199 (M199; #22340-020; Invitrogen) in a humidified atmosphere (95% air, 5% CO₂) at 37 °C. The culture medium contained Earle's salts, 25 mM HEPES, 5.5 mM D-glucose, 0.7 mM L-glutamine, 10% (v/v) fetal calf serum, 100 IU/ml penicillin and 100 IU/ml streptomycin.

2.4. SDS-PAGE and BN-PAGE analysis of brain slices, mouse embryonic fibroblasts (MEFs) and patient fibroblasts

Denaturing SDS-PAGE and blue-native-PAGE (BN-PAGE) followed by Western blotting were performed as described in the Supplement.

2.5. Data analysis, molecular graphics and protein homology structural modeling

Comparison of proteome data between brain slices of WT and KO animals was performed using the Benjamini-Hochberg (BH) procedure [45]. KO/WT protein ratios with a BH-P-value < 0.05 were considered to be significantly changed. Unless stated otherwise, all other data was compared using an independent Student's *t*-test. Averages are presented as mean ± SEM (standard error of the mean). Cluster analysis was performed using Ward's method and the Euclidian distance [46]. Statistical and cluster analyses were carried out using OriginPro software (OriginLab Corporation, Northampton, MA, USA). Molecular graphics were created using the PyMOL Molecular Graphics System Version 2.0 (Schrodinger-LLC, Mannheim, Germany). The homology model for *NDUFAF2* was generated using the Phyre² server (Protein Homology/analogy Recognition Engine V2.0; [47]) with default settings. The server used the cryo-EM model of *Yarrowia lipolytica* *NDUFAF2* (chain k in PDB 6RFQ). Ovine *NDUFAF2* is 32/44% identical/similar to ovine *NDUFA12* and 38/55% to *Yarrowia* *NDUFAF2*, so the structural model of the assembly factor in *Yarrowia* [14] represents a better starting model than the homologous ovine *NDUFA12* subunit. The generated homology model was aligned to *NDUFA12* subunit and thus placed in its location within the complex (PDB 5LNK), with all the subunits missing in the 830 kDa subcomplex removed.

3. Results

3.1. *Ndufs4* gene deletion reduces the protein levels of CI structural subunits and increases the levels of specific CI assembly factors in mouse tissues

To determine whether *Ndufs4* knockout affected the protein level of OXPHOS subunits and assembly factors, we performed a quantitative proteome analysis of mouse tissues (brain, heart, skeletal muscle, liver, kidney and diaphragm; Supplementary Fig. S1). Importantly, given the brain-specific phenotype in whole-body *Ndufs4* knockout (KO) mice (see Introduction) we focused our statistical data analysis on brain tissue (3 KO vs. 3 WT animals), to which the other tissues were compared (1 KO vs. 1 WT animal). In total, the relative protein expression level (KO/WT) of 86 different OXPHOS structural subunits was quantified (Fig. 1A; Supplementary Table S2). With the exception of *NDUFV3* and *NDUFAB1*, knockout of *Ndufs4* significantly reduced the levels of all CI structural proteins (Fig. 1A; marked in red characters). In contrast, *Ndufs4* knockout did not reduce the levels of other OXPHOS complex (CII-CV) subunits. With the exception of *NDUFAB1*, of which

CI contains two copies (α and β), all OXPHOS subunits occur only once in each OXPHOS complex. This allows determining the relative amount of each OXPHOS complex by calculating the average level (KO/WT) of its constituting subunits. In brain and diaphragm, *Ndufs4* knockout reduced the average CI subunit level by more than 60% relative to WT, whereas in liver, heart, kidney and skeletal muscle this reduction was significantly less (Fig. 1B; left panel). In case of CII, its average subunit level was not reduced in any of the tissues and significantly increased in heart and kidney (Fig. 1B; right panel). *Ndufs4* knockout did not generally affect the average subunit level of CIII, CIV and CV (Fig. 1C). Proteome analysis highlighted 34 OXPHOS assembly factors (Fig. 1D; Supplementary Table S2). Focusing on CI in the brain, *Ndufs4* gene deletion specifically increased the protein levels (KO/WT) of *NDUFAF1*, *NDUFAF2*, *ECSIT*, *ACAD9*, *FOXRED1* and *TMEM186* whereas it did not affect the levels of *NDUFAF3*, *NDUFAF4*, *NDUFAF5*, *NDUFAF6*, *NDUFAF7*, *NUBLP*, *TIMMDC1*, *TMEM70*, *TMEM126B* and *TMEM261*. Expression of assembly factors for other OXPHOS complexes was not affected in KO brain, except for the CV assembly factor *ATPAF2*, which also appeared increased in the other KO tissues (Fig. 1D). These results demonstrate that *Ndufs4* knockout reduces the level of CI subunits and increases the level of specific CI assembly factors.

3.2. *Ndufs4* gene deletion induces combined loss of *NDUFS4* and *NDUFA12* protein and increases *NDUFAF2* protein levels in mouse tissues

Focusing on CI, we next compared the expression level (KO/WT) of its structural subunits and assembly factors in brain with that of the other tissues (Fig. 2A). In general, protein levels in the brain (x-axis) correlated well with other tissues (y-axis; thick line: $y = x$). Cluster analysis highlighted four distinct groups (Fig. 2A; colored ovals). As expected, *Ndufs4* gene knockout induced a complete loss of *NDUFS4* protein in all KO tissues. However, this knockout also greatly reduced the levels of *NDUFA12* (Fig. 2A; pink oval). No *NDUFS4* peptide fragments were detected whereas *NDUFA12* fragments were virtually absent (Supplementary Fig. S2), which demonstrates that the overall level of this protein is greatly reduced. Relative to other CI subunits the reduction in brain *NDUFS4* and *NDUFA12* level was 12-fold larger. All KO mice tissues displayed reduced levels of CI structural subunits (Fig. 2A; purple oval), a moderate increase in various CI assembly factors (Fig. 2A; orange oval), and a 2-fold higher level of the CI assembly factor *NDUFAF2* (Fig. 2A; green oval). SDS-PAGE analysis of KO brain tissue yielded protein levels that correlated well with our proteome analysis, and confirmed that *NDUFS4* was absent, *NDUFA12* levels were greatly reduced and *NDUFAF2* was increased (Supplementary Fig. S3). Recent data suggests that functional CI is assembled via a mechanism in which five CI protein modules are pre-formed (N, Q/Pp-a, Pp-b, Pd-a and Pd-b) and subsequently combined [8]. Within the CI structure *NDUFS4* is localized close to the boundary between the N- and Q-module (Fig. 4A). Compatible with this localization, quantification of module-specific subunit expression levels (Supplementary Table S1) revealed that *Ndufs4* knockout reduces the average subunit level (KO/WT) of the N- and Q-module to a greater extent than that of the Pp- and Pd-module (Fig. 2B). Collectively, these results demonstrate that the complete absence of *NDUFS4* in all tissues is associated with: (i) near complete absence of *NDUFA12*, (ii) increased levels of *NDUFAF2*, and (iii) reduced stability of N- to Q-module attachment.

3.3. *Ndufs4* gene knockout is associated with an *NDUFAF2*-containing CI subassembly that incorporates into larger OXPHOS assemblies in mouse embryonic fibroblasts

To study the effects of *Ndufs4* gene knockout on CI assembly/stability, we analyzed mouse embryonic fibroblasts (MEFs) derived from WT and *Ndufs4*^{-/-} mice [40]. Supporting our proteomics results, *NDUFS4* was not detected, *NDUFA12* was greatly reduced and *NDUFAF2* was increased in KO-MEFs (Fig. 3A–B). To visualize the effect

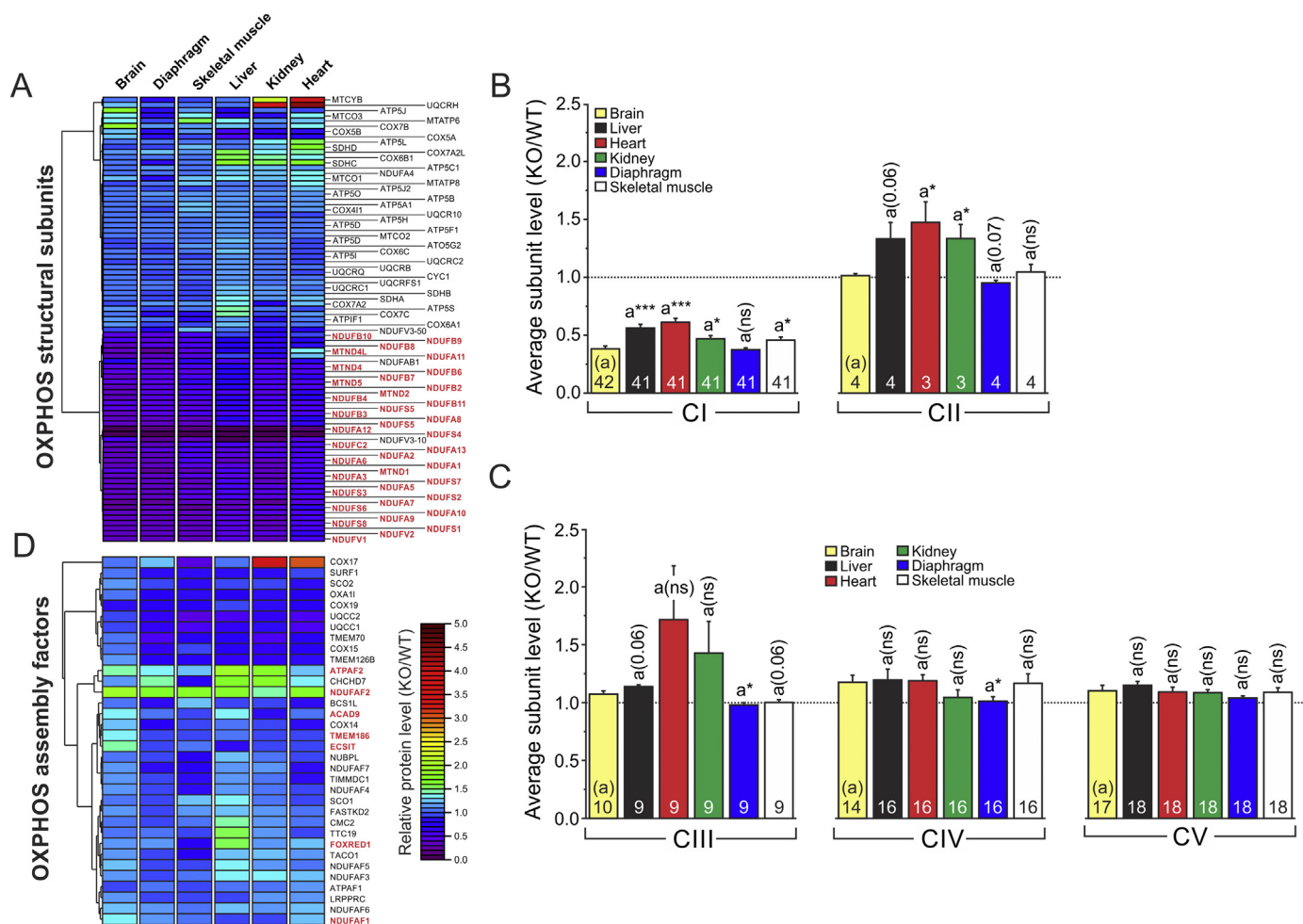


Fig. 1. OXPPOS proteome in brain, liver, heart, kidney, diaphragm and skeletal muscle for WT and KO animals. (A) Heatmap depicting the relative protein level (KO/WT) of OXPPOS structural subunits (y-axis) in various tissues (x-axis). The dendrogram depicts the result of a cluster analysis on OXPPOS structural subunits (y-axis). Proteins marked in red display a significantly different expression in KO brain (BH-P < 0.05). (B) Average subunit level (KO/WT) for CI and CII in the various tissues. Numerals indicate the number of subunits used to calculate the average level. (C) Correlation between the average subunit level (KO/WT) of CI (x-axis) and CII (y-axis) depicted in panel B. A significant linear correlation was observed (continuous line). Dotted lines mark the 95% confidence limits of the fitted line. (D) Same as panel B, but now for CIII, CIV and CV. (E) Same as panel A, but now for OXPPOS assembly factors. In panel B and D significant differences with brain (yellow column; marked ‘a’) are indicated: *P < 0.05, ***P < 0.001. For borderline significant differences the P-value is given. Non-significant differences are marked by ‘ns’.

of *Ndufs4* knockout on the levels of CI and its incorporation in OXPPOS assemblies of higher molecular weight, we performed blue native gel electrophoresis (BN-PAGE) of WT and KO MEFs (Fig. 3C). Given the reduction in N- and Q-module subunits in *Ndufs4*^{-/-} tissues (see above) we detected CI using an antibody against its NDUFA9 subunit, which is essential in stabilizing the junction between these modules [48]. This suggested that (Fig. 3C; “NDUFA9”) WT-MEFs contain a fully assembled “free” CI and a CI + CIII₂ assembly, whereas KO-MEFs contain a smaller CI subassembly of ~830-kDa in a free (“CI-830”) and CIII₂-attached form (“CI-830 + CIII₂”). In-gel activity (IGA) analysis demonstrated that CI was active in its free and CIII-bound form in WT-MEFs, whereas free and CIII₂-attached CI-830 were inactive in KO-MEFs (Fig. 3C; “IGA”). In WT-MEFs, low levels of NDUFAF2 were detected in two distinct bands associated with CI-830 (Fig. 3C; “NDUFAF2”). In KO-MEFs, NDUFAF2 levels were much higher than in WT-MEFs and localized in three distinct bands representing CI-830, CI-830 + CIII₂ and an even larger assembly potentially containing CIV (“CI-830-CIII₂-CIV?”). The latter assembly was not detected in WT-MEFs. These BN-PAGE results suggest that a large and parallel reduction in the levels of NDUFS4 and NDUFA12 stimulates association of NDUFAF2 with a catalytically inactive CI-830 subcomplex and that CI-830-NDUFAF2 is incorporated into larger assemblies.

3.4. The loss of *NDUFS4* greatly reduces *NDUFA12* protein levels in primary fibroblasts from patients with isolated CI deficiency

To determine the relevance of the findings mentioned above in human CI deficiency, we next compared the levels of NDUFS4, NDUFA12, NDUFAF2 and NDUFA9, as well as CI assembly/stability/IGA patterns, in fibroblasts from LS patients. These patient cells displayed an isolated CI deficiency and carried mutations in *NDUFS7*, *NDUFV1*, *NDUFA12*, *NDUFS1*, *NDUFS4* and *NDUFAF2* (Supplementary Table S1).

SDS-PAGE demonstrated that NDUFS4 was undetectable in patient cells with *NDUFS4* mutations, greatly reduced in cells with *NDUFS7*, *NDUFV1*, *NDUFS1* or *NDUFAF2* mutations, and not reduced in cells with an *NDUFA12* mutation (Fig. 3D). Confirming our results in *Ndufs4*^{-/-} mouse tissues and MEFs, NDUFA12 was not detected in cells from *NDUFS4* patients (Fig. 3E). For the other mutations, NDUFA12 was either not detected (*NDUFA12* patient cells) or reduced (*NDUFS7*, *NDUFV1*, *NDUFS1* patient cells). NDUFAF2 was not detected in *NDUFAF2* patient cells, slightly reduced in *NDUFA12* patient cells and not reduced in *NDUFS7*, *NDUFV1*, *NDUFS1* and *NDUFS4* patient cells (Fig. 3F). The levels of NDUFA9 were reduced in all cases except for *NDUFV1* patient cells (Fig. 3F).

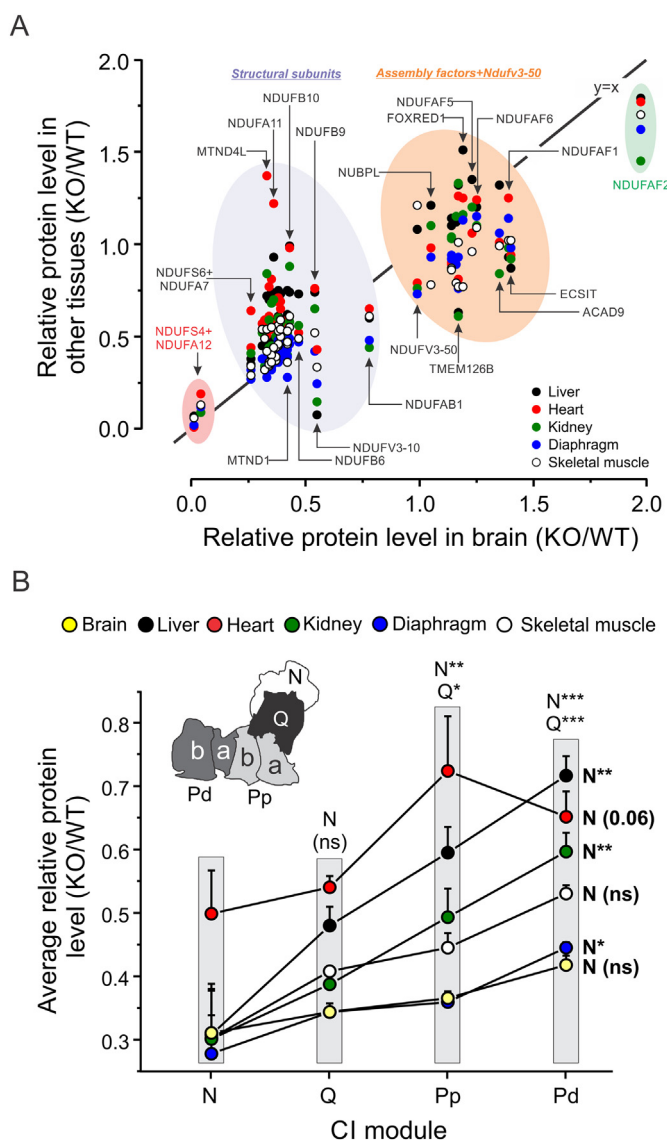


Fig. 2. CI proteome in brain, liver, heart, kidney, diaphragm and skeletal muscle for WT and KO animals. (A) Correlation between the relative protein level (KO/WT) of CI structural subunits and assembly factors in brain (x-axis) vs. other tissues (y-axis; colorized symbols reflect different tissues). Cluster analysis highlighted four distinct groups (highlighted ovals). (B) Average relative protein level (KO/WT) of the N, Q, Pp and Pd modules of CI, calculated by averaging the protein levels (KO/WT) of individual CI subunits that constitute these modules. The inset depicts the location of the modules within CI. Statistical comparisons between the protein level of the modules (KO/WT) were performed by comparing the average data for each module across tissues (significances marked in plain text on top), or by averaging protein levels (KO/WT) for each individual model in each tissue (significances marked in bold text on the right). Significant differences with the indicated modules (N,Q) are marked by: * $P < 0.05$, ** $P < 0.01$, *** $P < 0.001$.

Compatible with our results in *Ndufs4*^{-/-} MEFs, BN-PAGE demonstrated that *NDUFS4* patient cells contained a CI-830 subcomplex but no fully assembled CI (Fig. 3G; “NDUFA9”). In contrast, patient cells with an *NDUFV1*, *NDUFA12* or *NDUFS1* mutation contained both fully assembled CI and CI-830 (Fig. 3G; “NDUFA9”). Cells from the *NDUFS7* and *NDUFAF2* patients displayed a reduced level of fully assembled CI but no detectable amounts of CI-830 (Fig. 3G; “NDUFA9”). Compatible with SDS-PAGE analysis, *NDUFA12* was not detected in *NDUFS4* and *NDUFA12* patient cells at the height of fully assembled CI and variably reduced in the other patients (Fig. 3G; “NDUFA12”).

Although present in control and *NDUFS7* patient cells (Fig. 3F), *NDUFAF2* was not detected in the CI complex using BN-PAGE in these cells (Fig. 3G; “NDUFAF2”). In contrast, *NDUFAF2* was attached to the CI-830 subcomplex in *NDUFS4*, *NDUFS1* and *NDUFV1* patients. *NDUFA12* patient cells displayed an association of *NDUFAF2* with a catalytically active CI assembly (Fig. 3G; arrowheads). IGA analysis revealed that CI activity was reduced (*NDUFS1*, *NDUFS7*, *NDUFV1*, *NDUFA12*, *NDUFAF2*) or not detectable (*NDUFS4*) at the position of fully assembled CI (Fig. 3G; “IGA”). In addition, residual CI activity in *NDUFS4* patient cells was reduced more (i.e. to 7–14% of control) than in *NDUFA12* patient cells (42% of control; Supplementary Table S1).

Taken together, these results demonstrate that absence of *NDUFS4* due to *NDUFS4* mutations is associated with near complete loss of *NDUFA12* and increased levels of *NDUFAF2* in LS patient cells. We further observed that when *NDUFA12* is absent, the CI assembly factor *NDUFAF2* can replace this structural subunit in the presence of *NDUFS4* yielding catalytically active CI.

4. Discussion

Mutations in the *NDUFS4* gene, encoding an accessory subunit of mitochondrial complex I (CI), induce isolated CI deficiency and Leigh syndrome (LS) in pediatric patients. Using quantitative proteomics we here compared the level of OXPHOS subunits and assembly factors in tissues from *Ndufs4*^{-/-} mice. It was observed that *Ndufs4* knockout reduces CI subunit levels to a greater extent in brain and diaphragm relative to liver, heart, kidney and skeletal muscle (Fig. 1B). This result, combined with the fact that different organs display different thresholds below which an OXPHOS enzymatic deficiency induces pathology [49], suggests that the low CI subunit levels in brain, and possibly diaphragm, are responsible for the brain-specific clinical phenotype and breathing deficits in *Ndufs4*^{-/-} mice [31–35].

4.1. *Ndufs4* gene deletion does not reduce the level of *NDUFV3*, *NDUFAB1* and subunits of OXPHOS complexes II, III, IV and V

In case of the CI subunit *NDUFV3*, a 10-kDa (*NDUFV3-10*) and 50-kDa (*NDUFV3-50*) form were detected [50–52]. The number of peptides for *NDUFV3-10* and *NDUFV3-50* in the brain equaled 1 and 7, respectively. Therefore caution should be taken in the quantitative interpretation of the KO/WT ratio for *NDUFV3-10*, which was reduced to 0.5475 but did not reach quantitative significance. In the ovine CI structure only the *NDUFV3-10* form was detected (Fig. 4A), suggesting that *NDUFV3-10* is a genuine CI subunit whereas *NDUFV3-50* is not. Similar to *NDUFV3-10*, the KO/WT ratio for *NDUFAB1* (equaling 0.7804) appeared reduced relative to WT but this reduction was not statistically significant. This might be due to two copies of the *NDUFAB1* subunit being present in CI (Fig. 4A; α and β) and one of these being destabilized by the absence of *NDUFS4* to a greater or lesser extent. In addition, *NDUFAB1* can interact with other proteins including *LYRM2* and the mitochondrial ribosome-linked proteins *MALSU1* and *AltMid51* [53]. These interactions might stabilize and (partially) protect *NDUFAB1* from degradation under *NDUFS4*-deficient conditions. Although their functional role is still controversial [54], the structures of the CI + *CIII*₂ + *CIV* “supercomplex” and the *CI*₂ + *CIII*₂ + *CIV*₂ “megacomplex” were recently presented [13,16–18]. We observed that *Ndufs4*^{-/-} gene deletion greatly reduces CI subunit levels without lowering these levels for *CI*, *CIII*, *CIV* and *CV*. This argues against *in situ* structural stabilization of these complexes by CI in our experimental model.

4.2. *Ndufs4* gene deletion increases the level of specific CI assembly factors

In mouse brain, *Ndufs4* knockout was paralleled by an increase in the levels of specific CI assembly factors (*NDUFAF1*, *NDUFAF2*, *ECSIT*, *ACAD9*, *FOXRED1* and *TMEM186*), whereas the levels of *CI*, *CIII*, *CIV*

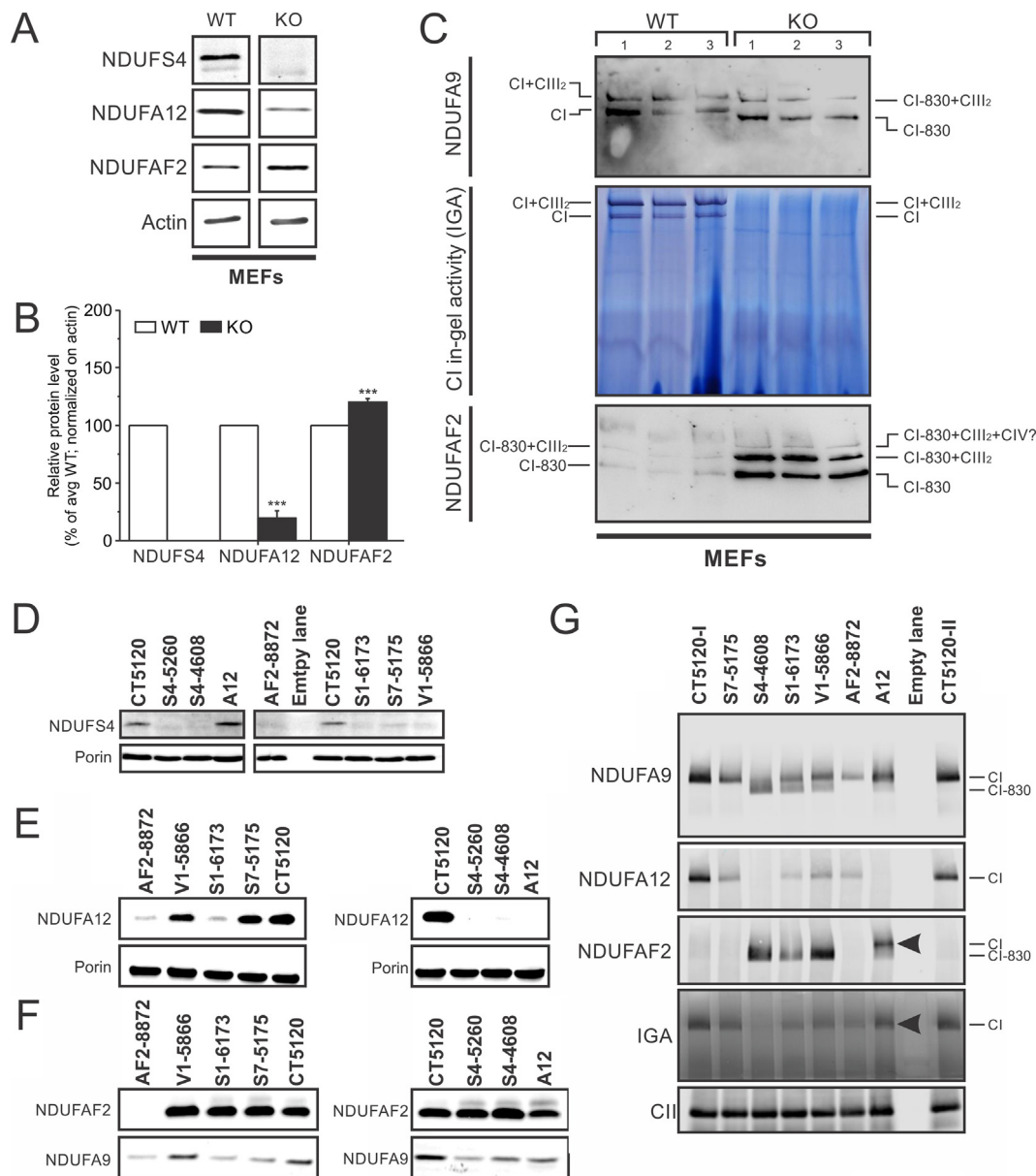


Fig. 3. SDS-PAGE and BN-PAGE analysis of mouse embryonic fibroblasts (MEFs) from WT and KO animals and Leigh Syndrome patients. (A) Protein level of NDUFS4, NDUFA12 and NDUFAF2 protein in whole cell homogenates from mouse embryonic fibroblasts (MEFs) derived from WT and KO animals. WT and KO bands were part of the same typical blot, which was contrast optimized for visualization purposes. (B) Average expression level of the proteins in panel A determined from the original, non-optimized, blots ($n = 3$ for both WT and KO). (C) Native gel (BN-PAGE) analysis of WT and KO MEFs (each in triplicate) depicting NDUFA9-positive bands (top panel), CI in gel activity (IGA; middle panel), and NDUFAF2-positive bands (lower panel). Bands are marked as follows: CI (representing fully assembled CI), CI + CIII₂ (representing the CI-CIII₂ supercomplex), CI-830 (representing the CI 830-kDa subcomplex), CI-830 + CIII₂ (representing the CIII-attached form of CI-830) and CI-830 + CIII₂ + CIV? (representing the CIII and potentially CIV-attached form of the CI 830-kDa subcomplex). (D–G) The patient cells carried mutations in *NDUFV1* (“V1-5866”), *NDUFS1* (“S1-6173”), *NDUFS4* (“S4-5260” and “S4-4608”), *NDUFS7* (“S7-5175”), *NDUFA12* (“A12”) and *NDUFAF2* (“AF2-8872”). For comparison a typical control cell line (“CT5120”) was included. (D) SDS-PAGE analysis of whole cell homogenates depicting the levels of NDUFS4 protein. Porin was used as a mitochondrial loading control. (E) Same as panel D but now for NDUFA12 protein. (F) Same as panel D but now for NDUFAF2 and NDUFA9 proteins using the same samples as in panel E. (G) Native gel (BN-PAGE) analysis of the patient cell lines (from top to bottom): NDUFA9 signal, NDUFA12 signal, NDUFAF2 signal, CI in-gel activity (IGA) signal and the level of CII (mitochondrial loading control). The positions of fully assembled CI and its 830-kDa subcomplex are marked by CI and CI-830, respectively. The arrowheads mark active CI with bound NDUFAF2. The control sample (CT5120) was included twice (marked I and II). The blots/gels in this figure were contrast optimized for visualization purposes. Statistics: relative to the WT condition: *** $P < 0.001$ (panel B).

and CV assembly factors were not affected. There was one exception to this pattern, the CV assembly factor ATPAF2 being increased in brain and the other KO tissues of the KO animals. This might suggest that ATPAF2 plays a role in CI assembly and/or stabilization. All of the above factors bound to CI assembly intermediates in 143B osteosarcoma cells [8]. NDUFAF1, ECSIT, ACAD9 and TMEM186 were present in a 357-kDa intermediate together with putative assembly factor COA1 (not detected in this study), assembly factor TMEM126b (not

altered in KO brain) and structural subunits MTND2, MTND3, NDUFC1 (not detected in this study) and NDUFC2. Later during CI assembly, MTND6 and MTND4L bind to the 357-kDa intermediate to form the Pp-b module [8]. The Pp-b intermediate subsequently combines with two structural subunits (NDUFA10 and NDUFS5) and the Pd-a module, which contains the structural subunits NDUFB1 (not detected in this study), NDUFB5, NDUFB6, NDUFB10, NDUFB11, MTND4 and the assembly factors TMEM70 (not altered in KO brain), FOXRED1 and

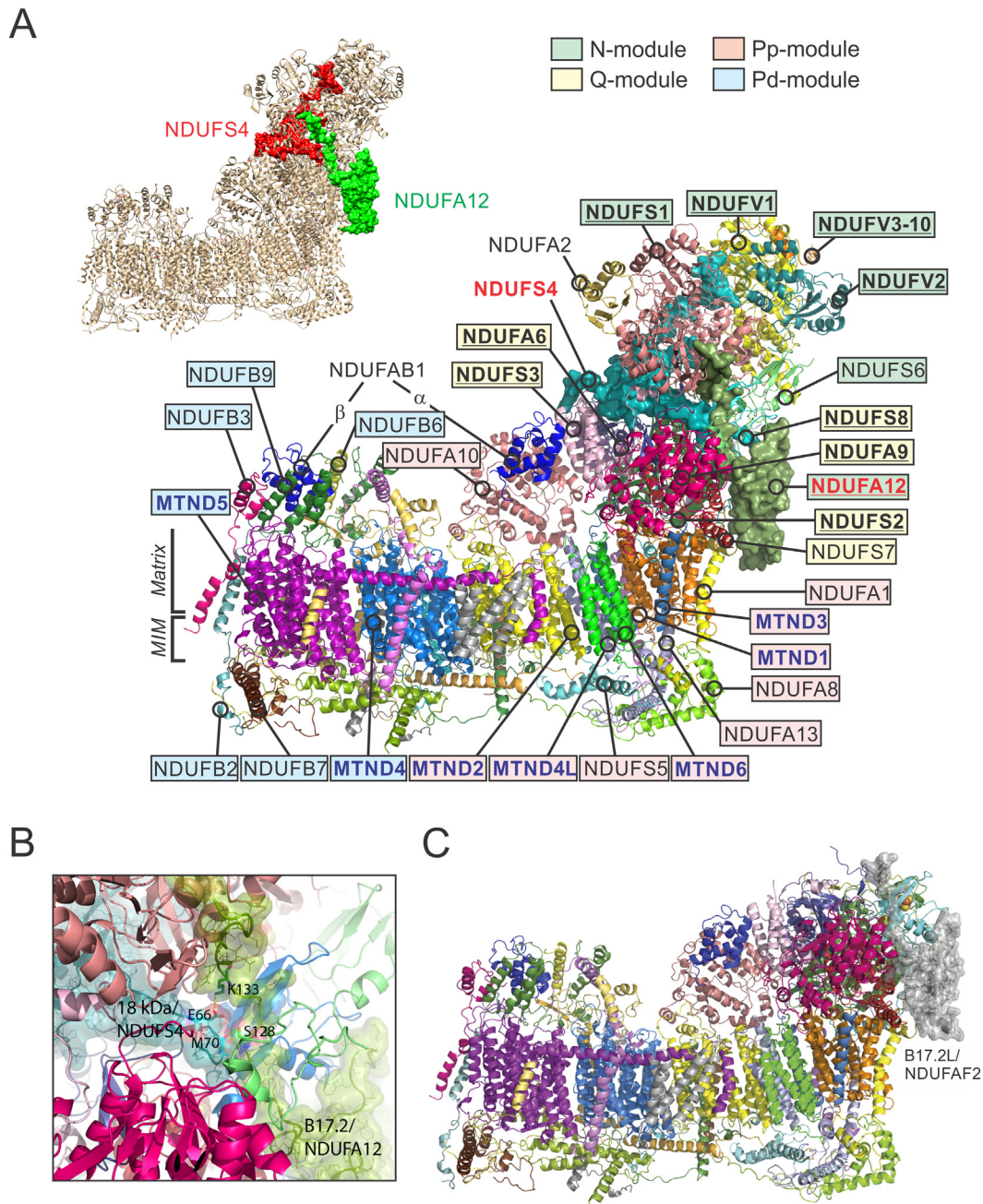
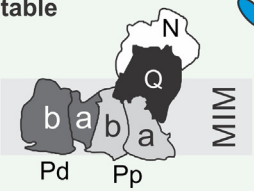
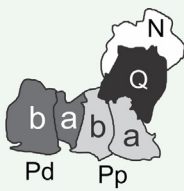
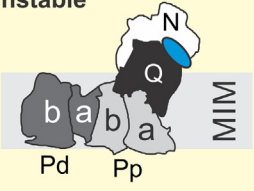
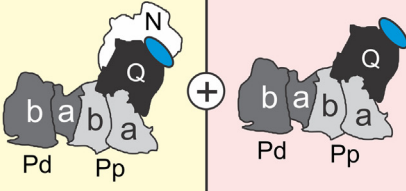
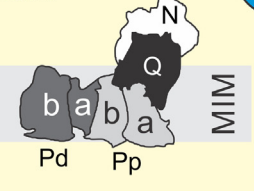
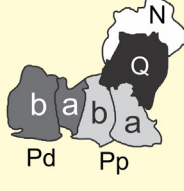
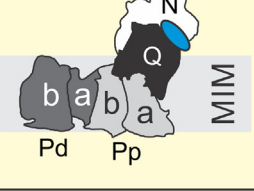
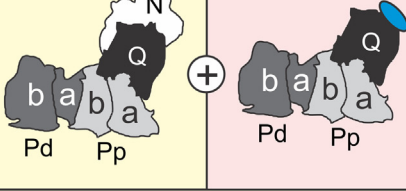
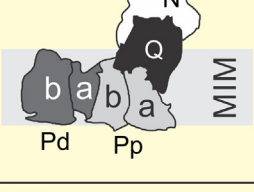
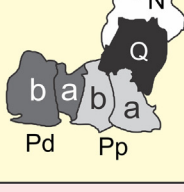
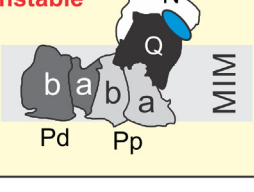
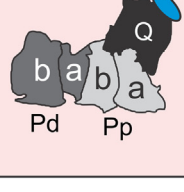


Fig. 4. Subunit localization, NDUF4-NDUFA12 interaction and NDUFAF2 homology modeling using the ovine CI structure. (A) Side view of *Ovis aries* heart CI cryo-EM structure (PDB accession number: 5LNK), embedded in the mitochondrial inner membrane (MIM) and highlighting the position of various structural subunits. The NDUF4 (red characters) and NDUFA12 (red underlined characters) subunits are depicted using a space-filling representation in cyan and green, respectively. NDUF4-interacting subunits (bold and underlined) and mtDNA-encoded subunits (bold and blue) are indicated. The assignment of subunits to various CI assembly modules is highlighted by different colors: N-module (green), Q-module (yellow), Pp-module (orange) and Pd-module (blue). The inset highlights the location of the NDUF4 and NDUFA12 subunit. (B) A surface rendering of NDUFA12 subunit (green; a.k.a. B17.2) and the NDUF4 subunit (cyan; a.k.a. 18-kDa) within the ovine CI structure. Residues making contacts between these two subunits are shown as sticks with putative hydrogen bonds are shown (yellow dots). These residues are conserved in mammals. (C) Probable binding of the NDUFAF2 assembly factor (a.k.a. B17.2L), illustrated using its homology model (space-filling, grey), to the putative 830-kDa CI subcomplex (which lacks its N-module, NDUFA12 and NDUF4).

ATP5SL (not altered in KO brain). Most assembly factors (except TMEM186 and COA1), dissociate from CI at the final stage of CI assembly [8]. Among the assembly factors, the level of NDUFAF2 was most highly increased in *Ndufs4* knockout brain. NDUFAF2 (a.k.a. NDUFA12L, Mimitin or B17.2L), a paralog of the NDUFA12 structural subunit of CI, plays a role during the final phase of CI assembly and insertion of FeS cluster N4 at the interface between the Q- and N-module [55–57].

4.3. *Ndufs4* gene deletion induces near complete loss of NDUFA12 and increases NDUFAF2

In addition to an increase in NDUFAF2, loss of NDUF4 was accompanied by near complete loss of NDUFA12 in *Ndufs4*^{-/-} mouse tissues, *Ndufs4*^{-/-} MEFs and NDUF4-mutated patient cells. In contrast, a similar loss of NDUFA12 was not observed in a mutated *Yarrowia lipolytica* strain lacking NDUF4 [14]. However, our mouse and human cell data is supported by studies in HEK293T cells [7],

| SDS-PAGE | <i>In situ</i> | BN-PAGE |
|-------------------------------------------------------------------------------------------------------------------------|---------------------------------------------------------------------------------------------------------------|---------------------------------------------------------------------------------------|
| CONTROL CELLS 100% NDUFS4 100% NDUFA12 100% NDUFAF2 | Stable  |  |
| NDUFA12 patient 215% NDUFS4 No NDUFA12 89% NDUFAF2 | Unstable  |  |
| NDUFS7 patient 34% NDUFS4 82% NDUFA12 121% NDUFAF2 | Stable  |  |
| NDUFV1/NDUFS1 patients 15/33% NDUFS4 74/11% NDUFA12 141/121% NDUFAF2 | Unstable  |  |
| NDUFAF2 patient 82% NDUFS4 8% NDUFA12 No NDUFAF2 | Stable  |  |
| Ndufs4^{-/-} mouse / NDUFS4 patients No NDUFS4 No NDUFA12 120/130% NDUFAF2 | Highly unstable  |  |

Normal activity
 Reduced activity
 No activity

Fig. 5. Integrated summary of results. Empirical data from SDS-PAGE, BN-PAGE and CI activity measurements was combined to deduce the *in situ* activity and stability of MIM-embedded CI in *Ndufs4*^{-/-} knockout tissues and LS patient cells with *NDUFA12*, *NDUFS7*, *NDUFV1*, *NDUFS2*, *NDUFAF2* and *NDUFS4* gene mutations. The relative cellular level of NDUFS4, NDUFA12 and NDUFAF2 is indicated in the column marked “SDS-PAGE”. The presence of assembled and active CI (CI) and the CI-830 subcomplex are indicated in the column marked “BN-PAGE” (see Discussion for details).

highlighting differences between yeast and mammalian cells/tissues. Inspection of the CI ovine and bovine cryo-EM structures [4,5], demonstrates that NDUFS4 and NDUFA12 physically interact and straddle the peripheral arm of CI from both sides, thereby linking its N and Q module (Fig. 4A–B). These studies also highlighted interactions between NDUFS4 and NDUFV1, NDUFV2 (not in bovine), NDUFV3–10,

NDUFS1, NDUFS2 (not in ovine), NDUFS3, NDUFS8, NDUFA6 and NDUFA9 (Fig. 4A; underlined subunits). All of these subunits are part of the N- or Q-module, compatible with our observation that combined loss of NDUFS4/NDUFA12 reduces the levels of N- and Q-module subunits to a greater extent than the levels of Pp- and Pd-module subunits (Fig. 2B). In patient cells, the absence of NDUFA12 was not

paralleled by reduced NDUFS4 levels. This suggests that NDUFS4 stabilizes NDUFA12 but not *vice versa*, and that the presence of NDUFS4 is more relevant for N- to Q-module attachment than NDUFA12.

Interestingly, studies in *Yarrowia lipolytica* revealed that deletion of the *NUMM* (*NDUFS6* homolog) gene, which encodes the NUMM/NDUFS6 accessory subunit of CI, blocks a late step in CI assembly [58]. In this model system, *NUMM/NDUFS6* gene deletion was associated with assembly of all CI core/accessory subunits except N7BM (NDUFA12 homolog), and firm association of N7BML (NDUFAF2 homolog) with a CI assembly intermediate. It was concluded that N7BM/NDUFA12 replaces N7BML/NDUFAF2 during complex I biogenesis [58]. The recently published cryo-EM structure from complex I obtained from a mutant *Yarrowia lipolytica* strain lacking NDUFS6 supports these findings [14]. Previous analysis of patient cells demonstrated that the absence of NDUFS4 and NDUFS6 induced formation of an 800-kDa subcomplex to which NDUFAF2 was attached [55–57]. The latter and our current findings support a mechanism based on evidence in *Neurospora crassa*, which proposes that NDUFAF2 is bound to a late CI assembly intermediate and dissociates upon binding of an NDUFA12/NDUFS4/NDUFS6-containing “regulatory” module [59]. However, differences between yeast and mammals do exist, as exemplified by the fact that, in contrast to our studies in mammals (*Ndufs4*^{-/-} mouse model and patient cells), deletion of NDUFS4 does not lead to loss of NDUFA12 in *Yarrowia lipolytica* [14].

4.4. The NDUFAF2 assembly factor can function as a stabilizing structural CI subunit

Previous results suggest that NDUFAF2 can associate with CI-830 but not with fully assembled CI [55]. In contrast, evidence in an artificial HEK293 cell model demonstrated that *Ndufa12* knockout triggers association of NDUFAF2 with active CI that appeared fully assembled [7]. Analyzing *NDUFA12* patient cells, we here observed that NDUFAF2 associates with a catalytically active CI assembly, but only in the absence of NDUFA12 and presence of NDUFS4. Analysis of residual CI activity in mitochondria-enriched fractions (Supplementary Table S1) revealed that this activity is reduced to a greater extent in NDUFS4 patient cells than in *NDUFA12* patient cells. This suggests that NDUFAF2 supports the formation of a catalytically active CI in the absence of NDUFA12 protein, in agreement with the presented BN-PAGE data revealing a complex within the same size range as in control cells (Fig. 3G). However, the residual CI activity in *NDUFA12* mitochondria was 42% of control, whereas this activity was only 7–14% in the NDUFS4 patients. This suggests that rescue by NDUFAF2 is unable to fully restore CI catalytic activity. This provides first time evidence in a disease-model that NDUFAF2 can act as a stabilizing structural subunit by replacing NDUFA12. Homology modeling suggests how binding of NDUFAF2/B17.2 L to the CI-830 subcomplex in the absence of NDUFA12/B17.2 and NDUFS4 (18-kDa) subunit might occur (Fig. 4C). To model NDUFAF2, we used the structure of *Yarrowia lipolytica* NDUFAF2 that recently became available [14]. The helical extension of NDUFAF2 could sterically hinder the interaction of NDUFS6 with nascent CI. However, our findings demonstrate that the CI formed is active and migrates at as similar height in *NDUFA12* patient cells as in control cells (Fig. 3G). Therefore, we hypothesize that NDUFS6 is able to bind, though possibly more weakly, to a structure in which NDUFAF2 has replaced NDUFA12.

Importantly, tissues from *Ndufs4*^{-/-} mice [60] and fibroblasts from patients with *NDUFS4* mutations (Supplementary Table S1) still display substantial CI activity measured in mitochondria-enriched fractions. Moreover, although oxygen consumption in *Ndufs4*^{-/-} MEFs is lower than in WT-MEFs it is still acutely blocked by the CI inhibitor rotenone [40]. This demonstrates that the absence of an IGA signal in *Ndufs4*^{-/-} MEFs and *NDUFS4*-mutated patient fibroblasts during BN-PAGE analysis does not reflect the *in situ* condition within living cells (Fig. 5). In this sense, the fact that BN-PAGE of *NDUFV1*- and *NDUFS1* patient cells

highlighted both fully active CI and the inactive NDUFAF2-CI-830 subcomplex, strongly suggests that NDUFAF2 stabilizes active CI *in situ* (Fig. 5). This is compatible with previous studies in *NDUFV1* patient cells [55,56]. In *Neurospora*, knockout of NDUFS1 leads to NDUFAF2 binding to nascent CI [59]. In agreement with this model, we here demonstrate that NDUFAF2 binds to the CI-830 subcomplex in *NDUFS1* patient cells. In case of *NDUFS7* patient cells, BN-PAGE analysis revealed a reduced level of active CI but no NDUFAF2-CI-830 subcomplex (although SDS-PAGE demonstrated that NDUFAF2 was present; Fig. 5). This lack of NDUFAF2-CI-830 subcomplex agrees with our previous findings [56].

4.5. Summary and conclusions

Taken together, our results demonstrate that absence of NDUFS4 greatly reduces NDUFA12 levels but not *vice versa*. This suggests a mono-directional stabilization of NDUFA12 by NDUFS4. We further provide evidence that NDUFAF2 stabilizes functional CI in the absence of NDUFA12 and presence of NDUFS4. The fact that absence of NDUFAF2 did not induce formation of the CI-830 subcomplex but lowered the levels of assembled and active CI in *NDUFAF2* patient cells, supports such a stabilizing role and suggests that NDUFAF2 is not a true CI assembly factor but acts as a chaperone instead [61]. In the presence of NDUFS4, NDUFAF2-mediated joining is quite strong since no discrete CI subassemblies were observed in *NDUFA12*-mutated patient cells. Integrating our findings (Fig. 5) supports a mechanism in which NDUFAF2 stabilizes CI *in situ*, not only in the absence of NDUFS4 and/or NDUFA12, but also in patient cells with mutations in *NDUFV1* and *NDUFS1*. The absence of NDUFS4 was associated with activity of CI *in situ* but not on BN-PAGE, which revealed an inactive NDUFAF2-CI-830 subcomplex. This suggests that the impact of BN-PAGE solubilization detergents on the level of assembled and active CI depends on CI stability. In this sense, our results not only highlight the crucial role of NDUFS4 in CI stabilization but also demonstrate that NDUFAF2 is unable to maintain N- to Q-module attachment under BN-PAGE conditions. Supporting the latter hypothesis, we have demonstrated the presence of a detached (partial) N-module using BN-PAGE analysis of *Ndufs4*^{-/-} mouse tissues [60]. Since CI catalytic function requires N-to-Q module attachment, we hypothesize that additional mechanisms are involved to sustain CI *in situ* activity in *Ndufs4*^{-/-} cells. Though still poorly understood, it is well established that lipid composition affects the conformation and activity of membrane-embedded proteins [62]. Also assembly and/or stabilization of OXPHOS complexes critically depend on specific MIM lipids [63]. Therefore we propose a model in which both NDUFAF2 and MIM lipids play a role in keeping the N- and Q-module together in the dual absence of NDUFS4 and NDUFA12. In this context, it might be possible that tissue-specific differences in NDUFAF2-mediated CI stabilization and/or MIM lipid physicochemical properties underlie the significantly greater reduction in CI subunit level observed in brain and diaphragm of *Ndufs4*^{-/-} mice.

Declaration of competing interest

The authors declare the following financial interests/personal relationships which may be considered as potential competing interests:

- Jan A.M. Smeitink is the founder and CEO of the SME Khondrion B.V. (Nijmegen, The Netherlands).
- Werner J.H. Koopman is a scientific advisor of the SME Khondrion B.V. (Nijmegen, The Netherlands).
- The SME Khondrion B.V. had no involvement in the data collection, analysis and interpretation, writing of the manuscript, and in the decision to submit the manuscript for publication.

Acknowledgements

We thank L.M.P.E van Oppen and Dr. S. Grefte (Dept. of Biochemistry) for assistance with cell culture and tissue dissection.

Funding

This work was supported by the CSBR (Centres for Systems Biology Research) initiative from the “Nederlandse organisatie voor Wetenschappelijk Onderzoek” (NWO, The Dutch Research Council) (Grant: #CSBR09/013V) and the Polish National Science Centre (Grant: UMO-2014/15/B/NZ1/00490).

Author contributions

Merel J.W. Adjobo-Hermans: Formal analysis; Writing - review & editing, Ria de Haas: Investigation; Methodology; Writing - review & editing, Peter H.G.M. Willems: Writing - review & editing, Aleksandra Wojtala: Investigation; Validation, Sjenet E. van Emst-de Vries: Investigation; Validation, Jori A. Wagenaars: Investigation; Validation, Mariel van den Brand: Investigation, Richard J. Rodenburg: Methodology; Supervision; Writing - review & editing, Jan A.M. Smeitink: Writing - review & editing, Leo G. Nijtmans: Writing - review & editing, Leonid A. Sazanov: Methodology; Visualization; Writing - review & editing, Mariusz R. Wieckowski: Methodology; Supervision; Writing - review & editing and Werner J.H. Koopman: Conceptualization; Supervision; Formal analysis; Writing - original draft; Writing - review & editing.

Appendix A. Supplementary data

Supplementary data to this article can be found online at <https://doi.org/10.1016/j.bbabo.2020.148213>.

References

- J.A.M. Smeitink, L. van den Heuvel, S. DiMauro, The genetics and pathology of oxidative phosphorylation, *Nat. Rev. Genet.* 2 (2001) 342–352.
- P. Mitchell, Coupling of phosphorylation to electron and hydrogen transfer by a chemi-osmotic type of mechanism, *Nature* 191 (1961) 144–148.
- U. Brandt, Energy converting NADH:ubiquinone oxidoreductase (complex I), *Annu. Rev. Biochem.* 75 (2006) 69–92.
- K. Fiedorczuk, J.A. Letts, G. Degliesposti, K. Kaszuba, M. Skehel, L.A. Sazanov, Atomic structure of the entire mammalian mitochondrial complex I, *Nature* 538 (2016) 406–410.
- J. Zhu, K.R. Vinothkumar, J. Hirst, Structure of mammalian respiratory complex I, *Nature* 536 (2016) 354–358.
- L. Sánchez-Caballero, S. Guerrero-Castillo, L. Nijtmans, Unraveling the complexity of mitochondrial complex I assembly: a dynamic process, *Biochim. Biophys. Acta* 1857 (2016) 980–990.
- D.A. Stroud, E.E. Surgenor, L.E. Formosa, B. Reljic, A.E. Frazier, M.G. Dibley, L.D. Osellame, T. Stait, T.H. Beilharz, D.R. Thorburn, A. Salim, M.T. Ryan, Accessory subunits are integral for assembly and function of human mitochondrial complex I, *Nature* 538 (2016) 123–126.
- S. Guerrero-Castillo, F. Baertling, D. Kownatzki, H.J. Wessels, S. Arnold, U. Brandt, L.G.J. Nijtmans, The assembly pathway of mitochondrial respiratory chain complex I, *Cell Metab.* 25 (2016) 128–139.
- R. Baradaran, J.M. Berrisford, G.S. Minhas, L.A. Sazanov, Crystal structure of the entire respiratory complex I, *Nature* 494 (2013) 443–448.
- C. Hunte, V. Zickermann, U. Brandt, Functional modules and structural basis of conformational coupling in mitochondrial complex I, *Science* 329 (2010) 448–451.
- K.R. Vinothkumar, J. Zhu, J. Hirst, Architecture of mammalian respiratory complex I, *Nature* 515 (2014) 80–84.
- V. Zickermann, C. Wirth, H. Nasiri, K. Siegmund, H. Schwalbe, C. Hunte, U. Brandt, Structural biology. Mechanistic insight from the crystal structure of mitochondrial complex I, *Science* 347 (2015) 44–49.
- J. Gu, M. Wu, R. Guo, K. Yan, J. Lei, N. Gao, M. Yang, The architecture of the mammalian respirasome, *Nature* 537 (2016) 639–643.
- K. Parey, O. Haapanen, V. Sharma, H. Köfeler, T. Züllig, S. Prinz, K. Siegmund, I. Wittig, D.J. Mills, J. Vonck, W. Kühlbrandt, V. Zickermann, High-resolution cryo-EM structures of respiratory complex I: mechanism, assembly, and disease, *Sci. Adv.* 5 (2019) eaax9484.
- G. Lenaz, G. Tioli, A.I. Falasca, M.L. Genova, Complex I function in mitochondrial supercomplexes, *Biochim. Biophys. Acta* 1857 (2016) 991–1000.
- J.A. Letts, K. Fiedorczuk, L.A. Sazanov, The architecture of respiratory supercomplexes, *Nature* 537 (2016) 644–648.
- M. Wu, J. Gu, R. Guo, Y. Huang, M. Yang, Structure of mammalian respiratory supercomplex I₁III₂IV₁, *Cell* 167 (2016) 1598–1609.
- R. Guo, S. Zong, M. Wu, J. Gu, M. Yang, Architecture of human mitochondrial respiratory megacomplex I₂III₂IV₂, *Cell* 170 (2017) 1247–1257.
- J.A. Letts, L.A. Sazanov, Clarifying the supercomplex: the higher-order organization of the mitochondrial electron transport chain, *Nat. Struct. Mol. Biol.* 24 (2017) 800–808.
- G.S. Gorman, P.F. Chinnery, S. DiMauro, M. Hirano, Y. Koga, R. McFarland, A. Suomalainen, D.R. Thorburn, M. Zeviani, D.M. Turnbull, Mitochondrial diseases, *Nat. Rev. Dis. Primers* 2 (2016) 16080.
- R.J. Rodenburg, Mitochondrial complex I-linked disease, *Biochim. Biophys. Acta* 1857 (2016) 938–945.
- F. Baertling, R.J. Rodenburg, J. Schaper, J.A.M. Smeitink, W.J.H. Koopman, E. Mayatepek, E. Morava, F. Distelmaier, A guide to diagnosis and treatment of Leigh syndrome, *J. Neurol. Neurosurg. Psychiatry* 85 (2014) 257–265.
- S. Scacco, V. Petruzzella, S. Budde, R. Vergari, R. Tamborra, D. Panelli, L.P. van den Heuvel, J.A. Smeitink, S. Papa, Pathological mutations of the human *NDUFS4* gene of the 18-kDa (AQDQ) subunit of complex I affect the expression of the protein and the assembly and function of the complex, *J. Biol. Chem.* 278 (2003) 44161–44167.
- C. Ugalde, R.J. Janssen, L.P. van den Heuvel, J.A. Smeitink, L.G. Nijtmans, Differences in assembly or stability of complex I and other mitochondrial OXPHOS complexes in inherited complex I deficiency, *Hum. Mol. Genet.* 13 (2004) 659–667.
- F. Valsecchi, W.J.H. Koopman, G.R. Manjeri, R.J. Rodenburg, J.A.M. Smeitink, P.H.G.M. Willems, Complex I disorders: causes, mechanisms and development of treatment strategies at the cellular level, *Development. Disab. Res. Rev.* 16 (2010) 175–182.
- S. Papa, D.D. Rasmø, Z. Technikova-Dobrova, D. Panelli, A. Signorile, S. Scacco, V. Petruzzella, F. Papa, G. Palmisano, A. Gnoni, L. Micelli, A.M. Sardaneli, Respiratory chain complex I, a main regulatory target of the cAMP/PKA pathway is defective in different human diseases, *FEBS Lett.* 586 (2012) 568–577.
- F. Kahlhöfer, K. Kmita, I. Wittig, K. Zwickler, V. Zickermann, Accessory subunit NUYM (NDUFS4) is required for stability of the electron input module and activity of mitochondrial complex I, *Biochim. Biophys. Acta Bioenerg.* 1858 (2017) 175–181.
- J.D. Ortigoza-Escobar, A. Oyarzabal, R. Montero, R. Artuch, C. Jou, C. Jiménez, L. Gort, P. Briones, J. Muchart, E. López-Gallardo, S. Emperador, E.R. Pesini, J. Montoya, B. Pérez, P. Rodríguez-Pombo, B. Pérez-Dueñas, Ndufs4 related Leigh syndrome: a case report and review of the literature, *Mitochondrion* 28 (2016) 73–78.
- P. Roestenberger, G.R. Manjeri, F. Valsecchi, J.A.M. Smeitink, P.H.G.M. Willems, W.J.H. Koopman, Mini-review: pharmacological targeting of complex I deficiency: the cellular level and beyond, *Mitochondrion* 12 (2012) 57–65.
- R. de Haas, D. Das, A. Garanto, H.G. Renkema, R. Greupink, P. van den Broek, J. Pertijs, R.W.J. Collin, P.H.G.M. Willems, J. Beyrath, A. Heerschap, F.G. Russel, J.A.M. Smeitink, Therapeutic effects of the mitochondrial ROS-redox modulator KH176 in a mammalian model of Leigh Disease, *Sci. Rep.* 7 (2017) 11733.
- S.E. Kruse, W.C. Watt, D.J. Marcinek, R.P. Kapur, K.A. Schenkman, R.D. Palmiter, Mice with mitochondrial complex I deficiency develop a fatal encephalomyopathy, *Cell Metab.* 7 (2008) 312–320.
- W.S. Choi, S.E. Kruse, R.D. Palmiter, Z. Xia, Mitochondrial complex I inhibition is not required for dopaminergic neuron death induced by rotenone, MPP⁺, or paraquat, *Proc. Natl. Acad. Sci. U. S. A.* 105 (2008) 15136–15141.
- W.S. Choi, R.D. Palmiter, Z. Xia, Loss of mitochondrial complex I activity potentiates dopamine neuron death induced by microtubule dysfunction in a Parkinson's disease model, *J. Cell Biol.* 192 (2011) 873–882.
- A. Quintana, S.E. Kruse, R.P. Kapur, E. Sanz, R.D. Palmiter, Complex I deficiency due to loss of Ndufs4 in the brain results in progressive encephalopathy resembling Leigh syndrome, *Proc. Natl. Acad. Sci. U. S. A.* 107 (2010) 10996–101001.
- A. Quintana, S. Zanella, H. Koch, S.E. Kruse, D. Lee, J.M. Ramirez, R.D. Palmiter, Fatal breathing dysfunction in a mouse model of Leigh syndrome, *J. Clin. Invest.* 122 (2012) 2359–2368.
- F.H. Sterky, A.F. Hoffman, D. Milenkovic, B. Bao, A. Paganelli, D. Edgar, R. Wibom, C.R. Lupica, L. Olson, N.G. Larsson, Altered dopamine metabolism and increased vulnerability to MPTP in mice with partial deficiency of mitochondrial complex I in dopamine neurons, *Hum. Mol. Genet.* 21 (2012) 1078–1089.
- G. Karamanlidis, C.F. Lee, L. Garcia-Menendez, S.C. Kolwicz Jr., W. Suthamarak, G. Gong, M.M. Sedensky, P.G. Morgan, W. Wang, R. Tian, Mitochondrial complex I deficiency increases protein acetylation and accelerates heart failure, *Cell Metab.* 18 (2013) 239–250.
- M.E. Breuer, P.H.G.M. Willems, W.J.H. Koopman, M. Nooteboom, Examining the validity of in vitro and in vivo models for *Ndufs4* mutations in respiratory complex I, *IUBMB Life* 65 (2013) 202–208.
- R. de Haas, F.G. Russel, J.A.M. Smeitink, Gait analysis in a mouse model resembling Leigh disease, *Behav. Brain Res.* 296 (2016) 191–198.
- F. Valsecchi, C. Monge, M. Forkink, A.J.C. de Groof, G. Benard, R. Rossignol, H.G. Swarts, S.E. van Emst-de Vries, R.J. Rodenburg, M.A. Calvaruso, L.G.J. Nijtmans, B. Heeman, P. Roestenberger, B. Wieringa, J.A.M. Smeitink, W.J.H. Koopman, P.H.G.M. Willems, Metabolic consequences of *Ndufs4* gene deletion in immortalized mouse embryonic fibroblasts, *Biochim. Biophys. Acta Bioenerg.* 1817 (2012) 1925–1936.
- W.J.H. Koopman, H.J. Visch, S. Verkaart, L.W. van den Heuvel, J.A.M. Smeitink, P.H.G.M. Willems, Mitochondrial network complexity and pathological decrease in complex I activity are tightly correlated in isolated human complex I deficiency, *Am. J. Phys. Cell Physiol.* 289 (2005) C881–C890.
- F. Distelmaier, H.J. Visch, J.A.M. Smeitink, E. Mayatepek, W.J.H. Koopman,

- P.H.G.M. Willems, The antioxidant Trolox restores mitochondrial membrane potential and Ca^{2+} -stimulated ATP production in human complex I deficiency, *J. Mol. Med.* 87 (2009) 515–522.
- [43] F. Distelmaier, W.J.H. Koopman, L.W. van den Heuvel, R.J. Rodenburg, E. Mayatepek, P.H.G.M. Willems, J.A.M. Smeitink, Mitochondrial complex I deficiency: from organelle dysfunction to clinical disease, *Brain* 132 (2009) 833–842.
- [44] P.H.G.M. Willems, J.A.M. Smeitink, W.J.H. Koopman, Mitochondrial dynamics in human NADH:oxidoreductase deficiency, *Int. J. Biochem. Cell Biol.* 41 (2009) 1773–1783.
- [45] Y. Benjamini, Y. Hochberg, Controlling the false discovery rate: a practical and powerful approach to multiple testing, *J. Royal Stat. Soc. B* 57 (1995) 289–300.
- [46] J.H. Ward Jr., Hierarchical grouping to optimize an objective function, *J. Am. Stat. Assoc.* 58 (1963) 236–244.
- [47] L.A. Kelley, S. Mezulis, C.M. Yates, M.N. Wass, M.J.E. Sternberg, The Phyre2 web portal for protein modeling, prediction and analysis, *Nat. Protoc.* 10 (2015) 845–858.
- [48] D.A. Stroud, L.E. Formosa, X.W. Wijeyeratne, T.N. Nguyen, M.T. Ryan, Gene knockout using transcription activator-like effector nucleases (TALENs) reveals that human NDUFA9 protein is essential for stabilizing the junction between membrane and matrix arms of complex I, *J. Biol. Chem.* 288 (2013) 1685–1690.
- [49] R. Rossignol, B. Faustin, C. Rocher, M. Malgat, J.P. Mazat, T. Letellier, Mitochondrial threshold effects, *Biochem. J.* 370 (2003) 751–762.
- [50] H.R. Bridges, K. Mohammed, M.E. Harbour, J. Hirst, Subunit NDUFV3 is present in two distinct isoforms in mammalian complex I, *Biochim. Biophys. Acta Bioenerg.* 1858 (3) (2017) 197–207.
- [51] M.G. Dibley, M.T. Ryan, D.A. Stroud, A novel isoform of the human mitochondrial complex I subunit NDUFV3, *FEBS Lett.* 591 (2017) 109–117.
- [52] S. Guerrero-Castillo, A. Cabrera-Orefice, M.A. Huynen, S. Arnold, Identification and evolutionary analysis of tissue-specific isoforms of mitochondrial complex I subunit NDUFV3, *Biochim. Biophys. Acta* 858 (2017) 208–217.
- [53] M.G. Dibley, L.E. Formosa, B. Lyu, B. Reljic, D. McGann, L. Muellner-Wong, F. Kraus, A.J. Sharpe, D.A. Stroud, M.T. Ryan, The mitochondrial acyl-carrier protein interaction network highlights important roles for LYRM family members in complex I and mitoribosome assembly, *Mol. Cell. Proteomics* 19 (2020) 65–77.
- [54] D. Milenkovic, J.N. Blaza, N.G. Larsson, J. Hirst, The enigma of the respiratory chain supercomplex, *Cell Metab.* 25 (2017) 765–776.
- [55] I. Ogilvie, N.G. Kennaway, E.A. Shoubridge, A molecular chaperone for mitochondrial complex I assembly is mutated in a progressive encephalopathy, *J. Clin. Invest.* 115 (2005) 2784–2792.
- [56] R.O. Vogel, M.A.M. van den Brand, R.J. Rodenburg, L.P.W.J. van den Heuvel, M. Tsuneoka, J.A.M. Smeitink, L.G.J. Nijtmans, Investigation of the complex I assembly chaperones B17.2L and NDUF1F1 in a cohort of CI deficient patients, *Mol. Genet. Metab.* 91 (2007) 176–182.
- [57] M. Lazarou, M. McKenzie, A. Ohtake, D.R. Thorburn, M.T. Ryan, Analysis of the assembly profiles for mitochondrial- and nuclear-DNA-encoded subunits into complex I, *Mol. Cell. Biol.* 27 (2007) 4228–4237.
- [58] K. Kmita, C. Wirth, J. Warnau, S. Guerrero-Castillo, C. Hunte, G. Hummer, V.R. Kaila, K. Zwicker, U. Brandt, V. Zickermann, Accessory NUMM (NDUFS6) subunit harbors a Zn-binding site and is essential for biogenesis of mitochondrial complex I, *Proc. Natl. Acad. Sci. U. S. A.* 112 (2015) 5685–5690.
- [59] B. Pereira, A. Videira, M. Duarte, Novel insights into the role of *Neurospora crassa* NDUF2, an evolutionarily conserved mitochondrial complex I assembly factor, *Mol. Cell. Biol.* 33 (2013) 2623–2634.
- [60] M.A. Calvaruso, P.H.G.M. Willems, M. van den Brand, F. Valsecchi, S. Kruse, R. Palmiter, J.A.M. Smeitink, L. Nijtmans, Mitochondrial complex III stabilizes complex I in the absence of NDUF4 to provide partial activity, *Hum. Mol. Genet.* 21 (2012) 115–120.
- [61] J.S. Schlehe, M.S. Journal, K.P. Taylor, K.D. Amodeo, M.J. LaVoie, The mitochondrial disease associated protein Ndufa2 is dispensable for complex-I assembly but critical for the regulation of oxidative stress, *Neurobiol. Dis.* 58 (2013) 57–67.
- [62] T. Harayama, H. Riezman, Understanding the diversity of membrane lipid composition, *Nat. Rev. Mol. Cell Biol.* 19 (2018) 281–296.
- [64] J.R. Nielson, J.P. Rutter, Lipid-mediated signals that regulate mitochondrial biology, *J. Biol. Chem.* 293 (2018) 7517–7521.